Three-Dimensional Structure at the Base of the Mantle Beneath the Central Pacific

Ludovic Bréger* and Barbara Romanowicz

Forward modeling of differential travel times of phases sensitive to lowermost mantle beneath the central Pacific reveals lateral heterogeneity that is higher in amplitude than predicted by tomographic models. A broad zone of low S velocity (−4 percent with respect to standard models), which may correspond to the base of a thermal "plume," narrows and is deflected as it extends to about 1000 kilometers above the core-mantle boundary. To the east of this zone, a localized region of fast S velocity (+5 percent) suggests strong heterogeneity or anisotropy related to the presence of high pressure and temperature assemblages, which may or may not involve core material. Its presence could also explain the observation of precursors to core reflected phases in this region.

The D″ region in the lowermost mantle (2600 to 2889 km deep) is a thermal and chemical boundary layer thought to play a critical role in the dynamics of Earth. Seismic body wave studies reveal a complex velocity structure (*1*). To explain observations of precursors to *ScS* phases, one-dimensional models involving a discontinuity at the top of D″ have been proposed, which are associated with variable vertical velocity gradients (*2*). On the other hand, recent studies provide evidence for the existence of strong lateral heterogeneity and anisotropy near the core-mantle boundary (CMB) (*3–10*).

It has also been proposed that *ScS* precursors might be a manifestation of complex three-dimensional (3D) structure rather than layering (*11*). Global tomographic models (*12, 13*) indicate a reddening of the spectrum of heterogeneity and an increase in the root mean square (rms) velocity fluctuations when approaching the CMB, but it has been shown that the lateral variations inferred within D″ by tomographic techniques are generally underestimated (*5, 6*). Characterization of two-dimensional (2D) and 3D heterogeneity near the CMB so far has been mostly qualitative and few studies have attempted 2D (*3, 10*), let alone 3D, forward modeling of body wave observations to quantitatively constrain the horizontal and vertical extent of prominent structures.

We assembled a data set of $S - SKS$ and $SKKS - SKS$ differential travel times for the central Pacific (Fig. 1A) and, by forward modeling, developed a family of local lowermost mantle models that provide good fits to these data. Our approach is to consider the variations with epicentral distance of $S - SKS$ and $SKKS - SKS$ travel time residuals computed with respect to preliminary reference Earth model (PREM) (*14*) for a fixed source or station and along narrow azimuthal corridors. This technique was used previously (*5, 6*) to document that strong lateral variations in S velocity must be locally present within D″. In particular, it was found that the location of velocity anomalies in the central Pacific was relatively well constrained by recent tomographic models (*12, 13*); however, these models underestimated the variations of observed residuals by a factor of 2 or 3. No modeling was attempted in these studies, and the results remained qualitative.

We have analyzed residuals for several large events in the Fiji-Tonga-Kermadec Islands region recorded at 111 North American stations (Fig. 1B) and for which the *SH* and *SV* radiations were favorable, which allowed the hand picking of *SKS*, *SKKS*, and *S* or *Sdiff* with an accuracy between 1 and 2 s (Fig. 2). By using differential travel times between *S* and *SKS*, or *SKS* and *SKKS*, we minimize errors due to source mislocation, uncertainty of earthquake origin times, and heterogeneity in the crust and upper mantle beneath sources and receivers. The 410 residuals collected were assembled into narrow azimuthal profiles. For different profiles corresponding to adjacent azimuths, residuals increase (Fig. 3, A, B, and E) or decrease (Fig. 3, C, D, and F) with increasing epicentral distance. This indicates a complex 3D velocity structure at a scale of several hundred kilometers at the base of the mantle. We ruled out contributions from the top 2000 km of the mantle for the following reasons: (i) In the upper 1000 km, raypaths of *S*, *SKS*, and *SKKS* are similar (Fig. 1A). To produce differential residuals varying by several seconds over less than 5° in epicentral distance would require unrealistically large anomalies in this depth range (larger than at least 10%), which is inconsistent with tomographic predictions. (ii) 3D tomographic models systematically indicate much lower rms amplitudes of lateral heterogeneity in the midmantle (1000 to 2000 km) than in the last 500 to 800 km of the lower mantle (*11, 12*). Explaining our observations mainly by midmantle heterogeneity would imply velocity anomalies in the midmantle of amplitude several times larger than in D″ and with shapes and signs that would be inconsistent with tomographic results. Overall, we estimate that the effect of 3D structure in the upper 2000 km can contribute at most 2 s to the observed differential travel times.

A one-dimensional model cannot account for the different trends observed in the residuals for adjacent azimuths and the same epicentral distance range. Although a 2D model would be sufficient to fit the data in a single azimuthal corridor, a 3D model is necessary to explain the observations over several azimuthal corridors. We chose a starting 3D model by computing predicted differential travel time residuals for several recent tomographic models (*12, 13*) and selecting the model that gave the closest match to the observed trends (model SAW12D) (*13*). Then, by forward modeling of travel time residuals (*15*), we progressively perturbed the

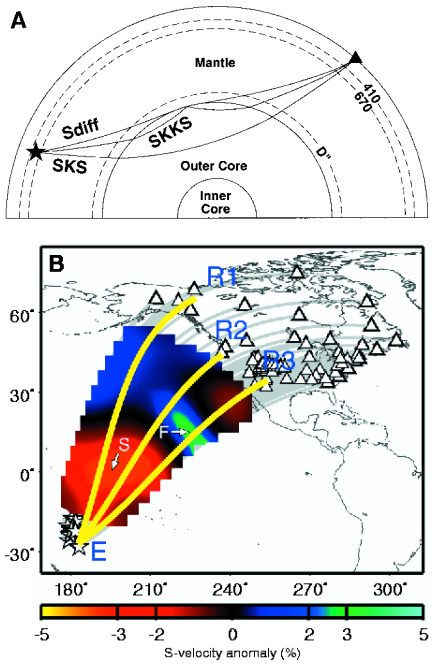

Fig. 1. (**A**) Schematic representation of the wavepaths of *SKS*, *SKKS*, and *Sdiff*. (**B**) Earthquakes (stars), stations (triangles), and projections of the raypaths (gray solid lines) used in the forward modeling presented in this study. We used 31 events from 1962 to 1998. Our data set consists of our own measurements and data from (*18*). Note the good coverage of the central Pacific. Paths E1-R1, E2-R2, and E3-R3 correspond to the depth cross sections presented in Fig. 5. Color contours correspond to our preferred S-velocity model for the region covered by our data set at 2700-km depth. Symbols S and F point to the slow and fast domains discussed in the text and also presented in the depth cross sections of Fig. 5.

Seismological Laboratory, University of California, Berkeley, CA 94720, USA.

*To whom correspondence should be addressed. E-mail: breger@seismo.berkeley.edu

starting model in two ways: (i) by preserving the spatial distribution of anomalies and modifying the amplitude of velocity fluctuations only in selected high- or low-velocity regions of the model and (ii) by slightly shifting them laterally when necessary to fit the observations. We found that lateral shifts on the order of less than 250 km were generally sufficient to fit the observations. By trial and error, we thus obtained a family of models capable of explaining not only the trends in the travel time versus distance plots but also the ranges of travel time fluctuations. We were able to achieve fits to all our data within 1 to 2 s (Figs. 3 and 4) which is within the accuracy of the travel time measurements.

Two prominent features are common to all models in the family (Figs. 1B and 5). A mild to strong increase of the $S - SKS$ residuals (Fig. 3, A and B) with epicentral distance is observed for a large number of events and azimuthal windows. This type of trend consistently requires a wide slow region at the bottom of the mantle south of Hawaii in the lowermost 1000 km of the mantle (S in Figs. 1B and 5). This anomalous region resembles that of the starting tomographic model in shape, but its amplitude needs to be increased to 3.5 to 4% throughout its domain (Figs. 1B and 5). For depths greater than 2000 km, the shape of the anomaly is well constrained by the 410 $S - SKS$ and $SKKS - SKS$ residuals. While narrowing with decreasing depth, the anomaly extends up to at least 1000 km above the CMB (*16*) with constant strength. Interestingly, another well-constrained feature is necessary to explain a different type of trend in the data, with rapidly decreasing residuals for distances between about 90° and 96° (Fig. 3, C and D). To explain these trends, it is necessary to introduce a fast region (F in Figs. 1B and 5C), adjacent to the large slow anomaly, where the velocity anomaly reaches +4 to 5% in a small domain that had only a mildly fast anomaly (about 1 to 2%) in the original model (Fig. 5, C and D). The exact shape and strength of these two required heterogeneous domains can vary slightly from one possible model to another but by no more than 100 to 200 km in position and 1% in amplitude. Besides these two localized heterogeneous regions, no significant modification to the initial tomographic model is necessary, at least in the domain sampled by our data set.

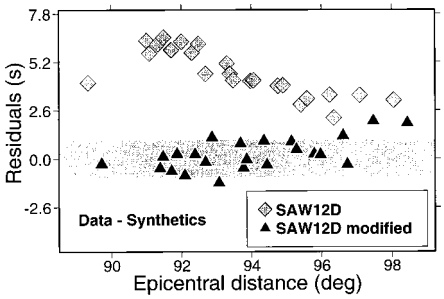

Fig. 4. Examples of differences between observed and predicted $S - SKS$ residuals for model SAW12D and for our preferred 3D model. Residuals are for event 92/06/25 (E in Fig. 1B). By amplifying the magnitude of heterogeneity in regions S and F (see Figs. 1B and 5), it is possible to improve the fit significantly.

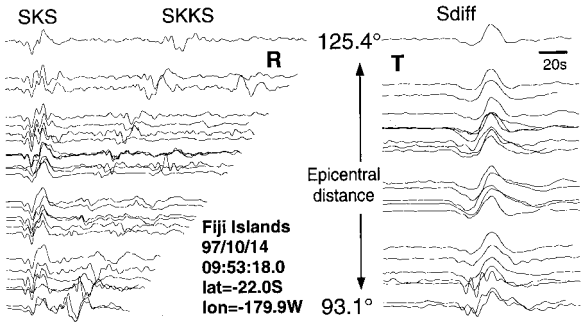

Fig. 2. Examples of records for event 97/10/14 and stations in North America. The azimuths considered are between 0° and 60°. R (radial) components are displayed on the left, and T (transverse) components are on the right. The similarity of the waveforms between *SKS* and *S*, and from one station to another, yields differential measurements with low scatter (Fig. 3A). We did not select data by narrow azimuthal corridors as in the study described in the text.

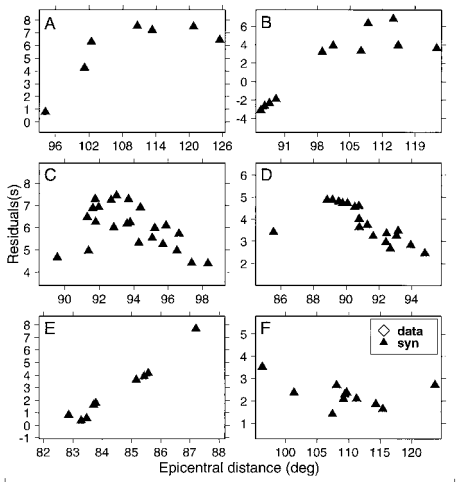

Fig. 3. Examples of observed variations of differential travel time residuals for $S - SKS$ as a function of epicentral distance (gray diamonds) along with synthetic predictions (black triangles) computed for our preferred 3D model. (**A** and **B**) Data and predicted residuals for events 97/10/14 and 98/03/29, respectively, and azimuths between 40° and 50°. S penetrates into the slow velocity region (see Fig. 4) as distance increases, and $S - SKS$ residuals correspondingly increase. (**C** and **D**) Same as (A) and (B) for events 92/06/25 and 92/07/11, respectively. The trend is opposite that observed in (A) and requires a fast region where the S-velocity anomaly reaches +5% (see Fig. 5). (**E**) $S - SKS$ residuals for fixed-station COR and several Fiji-Toga-Kermadec Islands events, and azimuths between 35° and 37°. (**F**) $SKKS - SKS$ residuals for event 98/03/29, and azimuths between 40° and 60°.

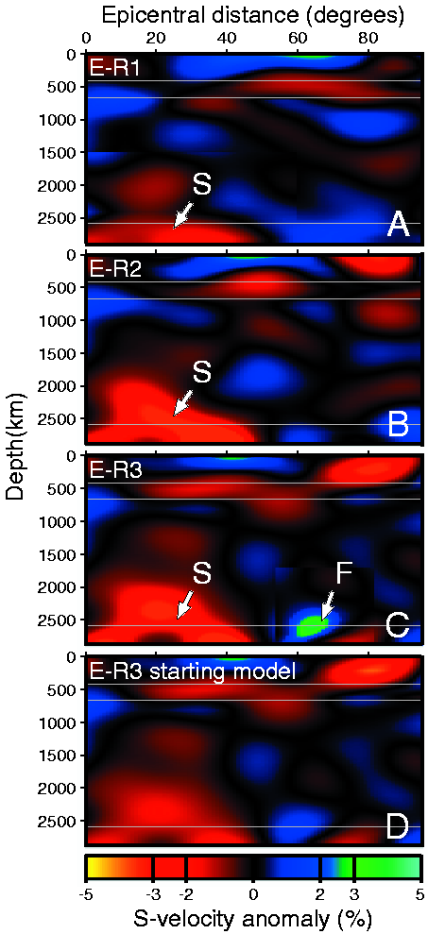

Fig. 5. Examples of vertical cross sections through our preferred model. (**A**) Vertical cross section through our preferred model for path E1-R1 (see Fig. 1B). A horizontal line was added at 410, 670, and 2600 km depth. (**B**) Same as (A) for path E2-R2. (**C**) Same as (A) for path E3-R3. The cross sections (A to C) show a velocity structure that depends strongly on the path chosen, which indicates a complex 3D structure. Note the presence of a large slow anomaly (S), where S velocity is reduced by about 3.5 to 4%, and of a smaller region (F), where it is increased by 4 to 5%. These two domains are required in all successful models in order to fit the travel time residual data. The fast velocity region (F) does not need to extend much above D″ and appears to be of smaller lateral extent than the "plume" region (S). However, our data set does not permit constraint where the anomaly ends to the southeast (Fig. 1B). (**D**) For comparison, vertical cross section through the starting model for path E3-R3, showing much lower amplitudes of lateral variations at the base of the mantle.

It has been proposed that the large slow region in the mantle beneath the central Pacific, identified in some early work (*3*) and observed in all tomographic models, is related to a megaplume generated by thermal boundary layer instabilities at the CMB (*17*). The large negative amplitude we infer in this region could be in part related to partial melt, as has been proposed to explain the ultralow velocities observed in some parts of this region (*18*). Some chemical heterogeneity, possibly involving core material, may be present as well (*19*). Our forward modeling predicts that the base of this possible upwelling is rather wide and that the plume narrows as it extends into the lower mantle, consistent with the spectral content of tomographic models, which shows a shift from red (large wavelengths) to white when ascending from the D″ region into the bulk lower mantle (*12, 13*). The plume also appears to be deflected to the southwest as it rises, indicating possible entrainment in the general circulation mantle flow (*20*).

The high-velocity region documented by our modeling represents a contrast of about 7 to 8% with respect to adjacent "hot" mantle and cannot be explained by thermal effects alone. A portion of ancient slab lying at the CMB is not likely to be responsible for this velocity contrast because reconstructions of ancient subduction zones do not predict the presence of remnant lithosphere in this part of D″ (*21*), and such a fossil slab might not produce a sufficient velocity contrast (*22*). This fast and localized anomaly could represent a high-velocity product of the decomposition of perovskite at temperatures and pressures corresponding to the lowermost mantle (*23*) or of core-mantle reactions (*19, 24*), and it may be related to the selective entrainment of chemically distinctive material into the thermal plume (*25*). Because significant shear wave splitting has been observed for waves traveling through that region (*6, 8*), the large velocity contrast that we have observed could also be related to anisotropy, whether it is due to lattice preferred orientation of anisotropic minerals (*24*) or laminar fabrics that would present themselves at different angles to the through-going SH waves, respectively, in the slow and fast regions. Finally, the block of fast material "sitting" on the CMB could be responsible for the intermittent reflections observed at the top of D″ in this region (*26*).

References and Notes

1. D. E. Loper and T. Lay, *J. Geophys. Res.* **100**, 6397 (1995).
2. T. Lay and D. V. Helmberger, *Geophys. J. R. Astron. Soc.* **75**, 799 (1983).
3. J. Schweitzer and G. Muller, *Geophys. Res. Lett.* **13**, 1529 (1986).
4. E. J. Garnero and D. V. Helmberger, *J. Geophys. Res.* **98**, 8225 (1993); M. Sylvander and A. Souriau, *Phys. Earth. Planet. Inter.* **94**, 1 (1996); M. E. Wysession, *Nature* **382**, 244 (1996); J. Ritsema, E. Garnero, T. Lay, *J. Geophys Res.* **102**, 20395 (1997).
5. L. Bréger, B. Romanowicz, L. Vinnik, *Geophys. Res. Lett.* **25**, 5 (1998).
6. L. Vinnik, L. Bréger, B. Romanowicz, *Nature* **393**, 564 (1998).
7. J. M. Kendall and P. G. Silver, *ibid.* **381**, 409 (1996).
8. J. Ritsema, E. J. Garnero, H. Benz, *Geophys. Res. Lett.* **25**, 1229 (1998).
9. J. E. Vidale and M. A. Hedlin, *Nature* **391**, 682 (1998).
10. L. Wen and D. V. Helmberger, *Science* **279**, 1701 (1998).
11. R. A. W. Haddon and G. G. R. Buchbinder, *Geophys. Res. Lett.* **14**, 891 (1987); V. F. Cormier, *J. Geophys.* **57**, 14 (1985); X. -F. Liu, J. Tromp, A. Dziewonski, *Earth Planet. Sci. Lett.*, in press.
12. S. Grand, R. van der Hilst, S. Widiyantoro, *G.S.A. Today* **7**, 1 (1997); X.-F. Liu, W.-J. Su, A. M. Dziewonski, *Eos (spring suppl.)* **75**, 232 (1994); G. Masters, S. Johnson, G. Laske, H. Bolton, *Philos. Trans. R. Soc. London* **354**, 1385 (1996).
13. X. -D. Li and B. Romanowicz, *J. Geophys Res.* **101**, 22245 (1996).
14. A. Dziewonski and D. L. Anderson, *Phys. Earth Planet. Int.* **25**, 297 (1981).
15. A finite difference (FD) modeling approach is desirable to forward model not only travel times but also waveforms in 3D. Such modeling is computationally heavy and not well suited for a trial and error approach unless the model space is restricted by using independent constraints. On the other hand, travel times can be modeled by using much more expedient ray approaches, which can provide well-constrained starting models for the more refined FD waveform modeling. We have computed synthetic travel time residuals for available tomographic models by using ray theory. The ray tracing was done in the spherically symmetric PREM model (*13*). We verified that, within the accuracy of the measurements (1 to 2 s), the results obtained for *S* and *SKS* were consistent with computations made with an acoustic 2D FD SH algorithm [J. E. Vidale, thesis, California Institute of Technology (1987)].
16. Large residuals (7 to 8s) are systematically observed at short distances (80° to 90°) on some profiles, implying very low velocities up to about 1000 km above the CMB. Tradeoffs between strength of anomalies and extent of the anomalous zone do not allow us to uniquely determine how much further above the CMB the anomaly extends. The model shown is, however, consistent with tomographic models, which show a significant drop in rms heterogeneity above that depth.
17. F. D. Stacey and D. E. Loper, *Phys. Earth. Planet. Inter.* **33**, 45 (1983); N. H. Sleep, *J. Geophys. Res.* **95**, 6715 (1990); P. F. Thompson and P. J. Tackley, *Geophys. Res. Lett.* **25**, 1999 (1998).
18. Q. Williams and E. J. Garnero, *Science* **273**, 1528 (1996).
19. E. Knittle and R. Jeanloz, *ibid.* **251**, 1438 (1991).
20. B. Steinberger and R. J. O'Connell, *Geophys. J. Int.* **132**, 412 (1998).
21. C. Lithgow-Bertelloni and M. A. Richards, *Rev. Geophys.* **36**, 27 (1998).
22. M. E. Wysession *et al.*, in *The Core-Mantle Boundary*, M. Gurnis, B. A. Buffett, E. Knittle, M. E. Wysession, Eds. (American Geophysical Union, Washington, DC, 1998), pp. 273–297.
23. L. S. Dubrovinsky *et al.*, *Nature* **388**, 362 (1998).
24. L. Stixrude, in *The Core-Mantle Boundary*, M. Gurnis, B. A. Buffett, E. Knittle, M. E. Wysession, Eds. (American Geophysical Union, Washington, DC, 1998), pp. 83–96; S. Karato, *Earth Space Sci.*, in press.
25. L. H. Kellogg and S. D. King, *Geophys. Res. Lett.* **20**, 379 (1993).
26. E. J. Garnero, D. V. Helmberger, G. Engen, *ibid.* **15**, 609 (1988).

27. We thank Ed Garnero for making his data available to us and for helpful discussions and two anonymous referees for constructive reviews. This work was funded by IGPP/LLNL grant 98-GS014. This is Seismological Laboratory contribution 98-04.

1 July 1998; accepted 15 September 1998

Pressure-Induced Landau-Type Transition in Stishovite

Denis Andrault,* Guillaume Fiquet, François Guyot, Michael Hanfland

A Rietveld structural analysis of stishovite, with angle-dispersive x-ray diffraction synchrotron source at the European Synchrotron Radiation Facility, confirmed a $CaCl_2$ form of stishovite distortion at 54 ± 1 gigapascals but confirmed no further phase transformation up to 120 gigapascals. The deviatoric stress that is usually encountered at such pressures was relaxed after yttrium-aluminum-garnet–laser heating. A single Birch-Murnaghan equation of state fits volumes of stishovite and a $CaCl_2$ form, showing that the tetragonal distortion occurs without a substantial change in volume. At the 54-gigapascal transition, the pressure-induced lattice modifications were similar to those found in a Landau-type temperature-induced transition. It is proposed that, above the transition pressure, the critical temperature increases above 300 kelvin, so that the lower entropy form becomes stable.

There is no closely packed compact ionic arrangement for metal dioxides. The most common dense form of BO_2 compounds (where B is Si, Ti, Ge, and so forth) is rutile, in which the oxygen sublattice can be seen as largely distorted face-centered cubic and in which only one of the two octahedral sites is filled by silicon (Fig. 1). Rutile can also be compared to the ABO_3 perovskite-type structure (where AB is MgSi, CaTi, SrZr, and so forth), in which the lack of the A cation would be balanced by a modification of the octahedral links, thus reducing the size of the vacant polyhedra. There are several other dense forms of the BO_2 compounds because

D. Andrault, Laboratoire des Géomatériaux, Institut de Physique du Globe, Paris 75252, France. G. Fiquet, Laboratoire de Géologie, Ecole Nationale Supérieure de Lyon, Lyon 69364, France. F. Guyot, Laboratoire de Minéralogie-Cristallographie, Université Paris VII, Paris 75252, France, and Institut de Physique du Globe, Paris 75252, France. M. Hanfland, European Synchrotron Radiation Facility, Grenoble 38043, France.

*To whom correspondence should be addressed.